

Stimulated Raman scattering produced by self-focusing in liquid crystals

P. Etchegoin* and R. T. Phillips

Cavendish Laboratory, University of Cambridge, Madingley Road, CB3 0HE, Cambridge, United Kingdom

(Received 21 March 1996)

The Raman spectra in backscattering and the far-field patterns of the transmitted light through a nematic liquid crystal cell are studied simultaneously. It is shown that stimulated Raman scattering is produced when self-focusing of the beam takes place. The threshold for stimulated scattering can be varied by selecting different angles between the polarization of the laser beam and the director orientation, thus changing the threshold for self-focusing. By using a microscope objective and focusing the input light to a beam waist of 10 μm we observe stimulated Raman scattering at very low powers (~ 8 mW) in a thin nematic film (~ 100 μm) for some orientations of the cell. The possibility of observing self-focusing and stimulated Raman scattering with low powers in a cavityless medium such as this is due to the extraordinarily large optical nonlinearities of liquid crystals in the nematic phase. [S1063-651X(96)02408-7]

PACS number(s): 61.30.Gd, 42.65.Dr, 42.65.Jx

I. INTRODUCTION

The nonlinear optical properties of liquid crystals have received considerable attention in the last 10–15 years [1,2]. The boost came from the early observations that liquid crystals have very large optical nonlinearities (about eight orders of magnitude larger than that of CS_2 , for example, and several orders of magnitude larger than anything accomplished so far in semiconductor microstructures) making them very suitable not only for the study of nonlinear optics but also for potential applications. A great many optical nonlinear processes have been observed to date in the different mesophases of liquid crystals [3]. To assemble a full list of references in this rapidly expanding field would be an impossible task [4]. We mention briefly, however, the most relevant nonlinear effects observed so far to convey a flavor of the present status in the field. Among the observed nonlinear optical phenomena we have [1] (i) self-focusing, self-defocusing, self-phase-modulation, optically induced molecular reorientation and light-induced Fréedericksz transitions [5–17]; (ii) degenerate and nondegenerate optical wave mixings (second and third harmonic generation, four wave mixing, etc.) [18–24]; (iii) stimulated scatterings of different types (thermal, Rayleigh wing, Brillouin) [25–30]; (iv) nonlinear waveguiding [31,32]; (v) optical bistability and all-optical switching [33–39], etc. A painstaking list of references of nonlinear optical effects in liquid crystals is given in the reviews by Khoo [2] and Jánossy [4].

In this paper, we are interested in one particular type of stimulated scattering, to wit: stimulated Raman scattering (SRS) [70]. We shall present measurements of SRS in a nematic liquid crystal cell of *N*-(*p*-methoxybenzylidene)-*p*-butylaniline (MBBA) [40] with planar orientation [1] at room temperature and demonstrate its relation with the occurrence of self-focusing. We show that the SRS threshold

can be obtained at very low powers of the order of a few mW for certain orientations of the nematic cell with respect to the laser polarization, bringing the phenomena of SRS and self-focusing in a cavityless medium such as this within the reach of a portable helium-neon laser. This is a natural consequence of the very large nonlinear optical constants of MBBA in the nematic phase as we shall explain in Sec. II.

The paper is organized as follows: Sec. II gives a general introduction to self-focusing due to molecular reorientation (in organic liquids and in liquid crystals in particular) as well as a brief description of previous Raman scattering experiments in MBBA and related nematics. The fundamentals of SRS are also given in Sec. II. In Sec. III we briefly present the experimental conditions and results. Finally, Sec. IV presents a brief discussion and discusses prospective directions of research.

II. GENERAL CONSIDERATIONS

Since we deal with self-focusing and SRS a brief introduction to both in the framework of liquid crystals is necessary for the sake of clarity.

A. Raman scattering

Raman scattering in liquid crystals has been used as a tool for probing the physical properties and the degree of order of the different mesophases since the early 1960's. A very important application came forward with the awareness that the Raman scattering selection rules could be used for retrieving information on the degree of order of the liquid crystalline mesophases [41–43]. A detailed comparison of the Raman spectra of the different mesophases of MBBA as a function of temperature has been given in Ref. [44].

It is a well-known fact in liquid crystals that an intense light beam may result in reorientation of the molecules [45] (see also next subsection). This is a spurious effect if one is aiming to evaluate the macroscopic order parameter produced by the orientation of the molecules in terms of polarization selection rules. Accordingly, Raman scattering experiments [46] are traditionally performed under low

*Permanent address: Centro Atómico Bariloche and Instituto Balseiro, Comisión Nacional de Energía Atómica and Universidad Nacional de Cuyo, 8400-San Carlos de Bariloche, Río Negro, Argentina.

excitation densities, in other words, under the conditions in which the presence of the laser light does not perturb the alignment imposed on a molecule by boundary conditions, temperature, and the internal molecular field of the nematic phase. In this way, maximum information about the degree of order of the liquid crystal can be obtained. The theory of Raman depolarization ratios in nematic liquid crystals has been thoroughly introduced in Refs. [41] and [42]. We therefore present a brief review of the main results. The Raman tensor for a particular vibration of interest (we ignore the rotational contribution [46] to the Raman scattering cross section in the nematic phase and consider only modes arising from internal vibrations) can be written for an elongated molecule as

$$\hat{R} = \alpha_0 \begin{pmatrix} a & 0 & 0 \\ 0 & b & 0 \\ 0 & 0 & 1 \end{pmatrix}. \quad (1)$$

Although the majority of the liquid crystal molecules are not strictly uniaxial (including MBBA) they can be fairly well approximated by a rodlike object in which the main axis of the tensor (1) coincides with the longest molecular axis \hat{z} . The scattering efficiency for a given selected pair of incident (\vec{e}_i) and scattered (\vec{e}_s) polarization vectors is given by $I \sim |\vec{e}_i \cdot \hat{R} \cdot \vec{e}_s|^2$ [46]. We define three depolarization ratios R_1 , R_2 , and R_3 as

$$R_1 = \frac{CI_{yz}}{I_{zz}}, \quad R_2 = \frac{I_{zy}}{CI_{yy}}, \quad R_3 = \frac{I_{yx}}{I_{xx}}, \quad (2)$$

with $C = [(n_w + n_e)/(n_w + n_o)]^2$ being n_e and n_o the extraordinary and ordinary refractive indices of the liquid crystal, respectively, and n_w the refractive index of the cell window. With the help of the additional definitions [in terms of the Raman polarizability components in (1)] $A = \text{Tr}(\hat{R}) = (1 + a + b)$, $B = (a - b)^2/4A^2$ and $D = (2 - a - b)/A$, the following system of equations is obtained [41,42]:

$$\frac{I_{xx}}{A^2} = \frac{1}{9} + \frac{3}{16}B + \frac{1}{18}D + \frac{11}{288}D^2 + \left(\frac{1}{8}B - \frac{1}{6}D - \frac{5}{48}D^2 \right) \langle \cos^2(\beta) \rangle + \left(\frac{3}{16}B + \frac{3}{32}D^2 \right) \langle \cos^4(\beta) \rangle;$$

$$\frac{I_{yx}}{A^2} = \frac{1}{16}B + \frac{1}{32}D^2 + \left(\frac{3}{8}B - \frac{1}{16}D^2 \right) \langle \cos^2(\beta) \rangle + \left(\frac{1}{16}B + \frac{1}{32}D^2 \right) \langle \cos^4(\beta) \rangle;$$

$$\frac{I_{zz}}{A^2} = \frac{1}{9} + \frac{1}{2}B - \frac{1}{9}D + \frac{1}{36}D^2 - \left(B - \frac{1}{3}D + \frac{1}{6}D^2 \right) \langle \cos^2(\beta) \rangle + \left(\frac{1}{2}B + \frac{1}{4}D^2 \right) \langle \cos^4(\beta) \rangle;$$

$$\frac{I_{yz}}{A^2} = \frac{1}{4}B + \frac{1}{8}D^2 \langle \cos^2(\beta) \rangle - \left(\frac{1}{4}B + \frac{1}{8}D^2 \right) \langle \cos^4(\beta) \rangle, \quad (3)$$

where β is the angle between the director orientation of the nematic and a fixed laboratory direction (taken along \hat{z} in this case). The brackets in $\langle \cos^2 \rangle$ and $\langle \cos^4 \rangle$ represent orientational averages for the nematic domain at fixed temperature without any effect from the laser. From the three quantities in (2) plus the depolarization ratio of the isotropic phase [46] R_{iso} we have four quantities to determine the four unknowns [41,42] a , b , $\langle \cos^2(\beta) \rangle$, $\langle \cos^4(\beta) \rangle$.

One way of evaluating the degree of molecular order in a liquid crystal is through the *scalar order parameter* S [3]. By taking the long axis (\hat{z}) of the molecule as a reference and calling \vec{n} the director orientation, S is defined by [3]

$$S = \frac{1}{2} \langle (\vec{n} \cdot \hat{z})^2 - 1 \rangle = \frac{1}{2} [3 \langle \cos^2(\beta) \rangle - 1]. \quad (4)$$

In fact, S is the first-order expansion of the orientational (angular) distribution function $f(\beta)$ (with axial symmetry along \hat{z} for a nematic) in terms of Legendre polynomials $P_{2l}(\cos(\beta))$,

$$\langle P_{2l}(\cos(\beta)) \rangle = \int_0^\pi f(\beta) P_{2l}(\cos\beta) \sin(\beta) d\beta, \quad (5)$$

so that $S = P_2$; $l=1$. The next order in the expansion of $f(\beta)$ would be

$$P_4 = \frac{1}{8} [35 \langle \cos^4(\beta) \rangle - 30 \langle \cos^2(\beta) \rangle]. \quad (6)$$

Inasmuch as both $\langle \cos^2(\beta) \rangle$ and $\langle \cos^4(\beta) \rangle$ are obtained through (3), information about the first- and second-order expansion terms of $f(\beta)$ can be gained with Raman scattering. This is a noteworthy characteristic of Raman spectroscopy that allowed [41] a more detailed comparison of experiments with accepted molecular models of the nematic phase such as the Maier-Saupe mean-field theory [45,47]. In addition, the technique can be advantageously used in combination with elongated dye guest molecules and resonant Raman scattering [43].

There are, however, several drawbacks to the method. Among them we mention the following: (i) the effects of local fields on the Raman results are debatable. Local field corrections are very important, if not dominant, in the optical properties (and electronic polarizabilities in general) of liquid crystals. A clear-cut theory on how to take them into account does not exist to date to our knowledge. In this respect, magnetic measurements are in general easier to interpret since local fields are negligible for them. (ii) The system of equations (3) can be slightly sensitive to small changes in parameters; and (iii) experiments performed in thick cells ($d \sim 200 \mu\text{m}$) show that the initial polarization of the laser is degraded along the path of the light beam. The reason for this scrambling of the polarization is the quasielastic scattering produced by the fluctuations of the director [48]. As a consequence, a Raman event produced deep in the cell has a different initial polarization \vec{e}_i and the depolarization ratios (2) are inaccurate. The problem is normally overcome by

measuring cells with different thicknesses and extrapolating to $d \rightarrow 0$, a procedure which requires some care.

Finally, a few words on SRS. We follow closely Refs. [45,49–51] in the presentation. The presence of the electric field of the light in a molecule induces small changes in the normal coordinates q of the molecular vibrations and therefore changes in the optical polarizabilities $\alpha(q)$ associated with the mode

$$\alpha(q) \sim \alpha_0(q_0) + \left[\frac{\partial \alpha(q)}{\partial q} \right]_{q_0} q, \quad (7)$$

which, in turn, produces an induced polarization \vec{P}_{ind} :

$$P_{\text{ind}} \sim \epsilon_0 q E \left[\frac{\partial \alpha(q)}{\partial q} \right]_{q_0} \left(\frac{N}{V} \right), \quad (8)$$

with N/V the density of molecules, and an interaction Hamiltonian given by

$$\hat{H}_R = -\vec{P}_{\text{ind}} \cdot \vec{E} = -\epsilon_0 \left[\frac{\partial \alpha(q)}{\partial q} \right]_{q_0} q \vec{E} \cdot \vec{E}. \quad (9)$$

The normal coordinate q responds to an equation of motion for a forced harmonic oscillator and is driven by $F = -\partial H_R / \partial q \sim E^2$. Hence, $q \sim E^2$ and $P_{\text{ind}} \sim E^3$; i.e., a third-order nonlinear polarizability is involved in the Raman process [49,50]. Calling the incident laser frequency ω_L , ω_q is the vibration energy of the Raman mode and ω_S the Stokes frequency of the scattered light ($\omega_S = \omega_L - \omega_q$) the nonlinear polarization associated with Stokes-Raman scattering will be of the form [45] $P \sim (E_{\omega_S} E_{\omega_L}^*) E_{\omega_L}$, i.e., given through a nonlinear optical term such as

$$P_{\text{ind}} \sim \chi_s^{(3)}(-\omega_S, \omega_L, -\omega_L, \omega_L) E(\omega_S) E^*(-\omega_L) E(\omega_L). \quad (10)$$

The correct way to solve the propagation of several waves in a nonlinear optical medium, taking into account the possible interactions and mixings among them, is to solve the coupled Maxwell wave equations with the corresponding phase matchings [45,50]. This is the common framework for the description of a variety of processes such as four wave mixing, second and third harmonic generations, optical phase conjugation, etc. The latter approach is normally not necessary in Raman scattering because both the Stokes and anti-Stokes fields are very weak in comparison with the laser and their coupling is negligible. It is, however, fundamental to understand the phenomenon of SRS. The amplitude of the Stokes field in the coupled Maxwell wave equations and in the slowly varying envelope approximation [45] (considering that $|E_S| \ll |E_L|$) becomes

$$\frac{\partial E_S}{\partial z} = (ig|E_L|^2 - \gamma)E_S, \quad (11)$$

where $g = \mu_0 \omega_S^2 \chi_s^{(3)} / 8k_S$, with k_S the wave vector of ω_S and $\chi_s^{(3)}$ the corresponding nonlinear optical susceptibility component from (10) (also called Raman susceptibility). The parameter γ is added phenomenologically to account for losses

due to random scatterings, fluctuations, residual absorption, etc. The nonlinear susceptibility $\chi_s^{(3)}$ will have in general both real and imaginary parts $\chi_s^{(3)} = \chi_s' - i\chi_s''$. The solution for E_S in (11) has an amplitude envelope given by

$$|E_S| \sim \exp \left[\left(\frac{\mu_0 \omega_S^2 \chi_s'' |E_L|^2}{8k_S} - \gamma \right) z \right], \quad (12)$$

and an oscillatory component governed by χ_s' . It is clear from (12) that the Stokes field will be either exponentially damped or increased depending on whether $(\mu_0 \omega_S^2 \chi_s'' |E_L|^2 / 8k_S - \gamma) < 0$ or > 0 . The second case represents the SRS condition and depends on the pump field density reaching the SRS threshold:

$$|E_L|^2 = 8\gamma k_S / \mu_0 \omega_S^2 \chi_s''. \quad (13)$$

Note that the larger the losses $\propto \gamma$ and the smaller the Raman susceptibility χ_s'' , the larger the intensity $I_L \sim |E_L|^2$ needed to produce SRS.

Stimulated Raman scattering is a phenomenon of pattern formation (or phase transition) outside equilibrium [52] and has all the characteristics of a threshold phenomenon such as the lasing of a cavity. In fact, the analogy with the lasing transition of a cavity is quite deep since Eq. (11) is very similar to the Van der Pol oscillator [53] (or overdamped harmonic oscillator), which governs the laser transition of a cavity [54]. It can also be put in terms of coupled rate equations for the number of pump and Stokes photons [49], even though information about the phases of the fields is lost in this approach.

B. Self-focusing

It is a well-established phenomenon in organic liquids that the SRS threshold obtained experimentally is much smaller than the one predicted by (13) [49,55–58]. The reason for this is self-focusing. In fact, the same nonlinear optical susceptibility responsible for SRS in (10) produces self-focusing of the pump beam, significantly increasing the effective power density. In general, the electric field strength achieved at the waist of the self-focused beam is enough to overcome the losses and SRS takes place at the threshold of self-focusing instead of (13). The effect comes through the mixing produced by the third-order nonlinear susceptibility as in (10) but with E_S replaced by E_L , i.e., the self-action of the beam through $\chi^{(3)}$. The easiest way to understand why self-focusing takes place is to realize that the existence of a polarizability $P \sim \chi^{(3)} E^3$ implies an intensity-dependent dielectric tensor $\epsilon_{ij}(\omega, \vec{E})$ of the form [49]

$$\epsilon_{ij}(\omega, \vec{E}) = \epsilon_{ij}^0 + \chi_{ijkl}^{(3)} E_k E_l. \quad (14)$$

Accordingly, assuming an incident Gaussian beam $E \sim E_0 \exp(-r^2/2\sigma^2) \exp(ik_L z)$, where $r^2 = (x^2 + y^2)$, the central part of the beam will experience a different index of refraction from that in the outer section. Depending on the sign of $\chi^{(3)}$ the central part of the beam will travel with an index of refraction $n(r=0)$, which can be larger or smaller than the one for $r \neq 0$. This is the principle of self-phase modulation. If $\chi^{(3)} > 0$, $n(r=0) > n(r \neq 0)$ and the beam cre-

ates its own waveguide. The waveguide tends to focus the beam towards the center and the higher the intensity at $r \sim 0$ the larger the waveguiding effect. This results in a self-driven process that collapses the beam to a small filament [50]. The size of the filament is a compromise between diffraction and the tendency of the medium to focus the intensity in the center. If $\chi^{(3)} < 0$ the beam self-defocuses.

In liquids formed by anisotropic molecules there is a natural mechanism to produce a quadratic index of refraction such as (14) [49] that does not exist in solids. The *orientational Kerr effect* is responsible for this contribution. Roughly speaking, the electric field of the light polarizes the molecule and creates a dynamic dipole proportional to E_L . This dynamic dipole interacts again with the laser producing a term proportional to E_L^2 , which strives to reorient the molecules to minimize the interaction energy. This nonlinearity exists irrespective of whether the liquid is in the isotropic, nematic, or smectic phase. It is well known, however, that this type of orientational nonlinearity can be enhanced by several orders of magnitude in the nematic with respect to the isotropic phase [2] and, in particular, close to the nematic-to-isotropic phase transition where critical slowing down of the molecules takes place [59]. The reorientational force produced by the light beam is caused by the optical torque [1]

$$\vec{M}_{\text{opt}} = C \langle (\vec{n} \cdot \vec{E}_L)(\vec{n} \times \vec{E}_L) \rangle, \quad (15)$$

where C is proportional to the dielectric anisotropy of the molecules $\Delta\epsilon = \epsilon_{\parallel} - \epsilon_{\perp}$. Equation (15) is zero if \vec{E}_L is exactly parallel or perpendicular to the director, albeit one of the two situations is energetically unstable depending on the sign of C . In an isotropic liquid, where the internal molecular field averages to zero, the tendency of the laser to reorient the molecules competes with temperature [49], which tends to randomize their orientations. In a nematic liquid crystal, in addition, an internal molecular field (responsible for the molecular order) exists and the laser-induced reorientation competes with the internal elastic energy of the nematic. The total free energy produced by the twist, bend, and splay [3] of the director plus the boundary conditions imposed by the walls of the cell wrestles with the laser-induced reorientation produced by (15). The optically induced torque has to overcome the internal elastic free energy and the quadratic nonlinearity in (14) appears only above a certain threshold. A situation similar to that found in ferromagnets with hysteresis is therefore accomplished. The external magnetic field struggles with the internal free energy imposed by the ferromagnetic domain walls. The macroscopic magnetization follows the external field only after a critical value has been reached. This is called the optical Fréedericksz transition in liquid crystals. The critical field for the Fréedericksz transition depends on the polarization of the incident beam with respect to the director, because this modifies the effectiveness of the torque (15).

Once the quadratic term in (14) above the Fréedericksz transition emerges, nematic liquid crystals display a fairly large nonlinearity. The far-field diffracted pattern of the self-focused beam in a medium with a quadratic nonlinearity is very difficult to calculate if the sample is thick and numerical solutions are almost always the rule. For thin samples, how-

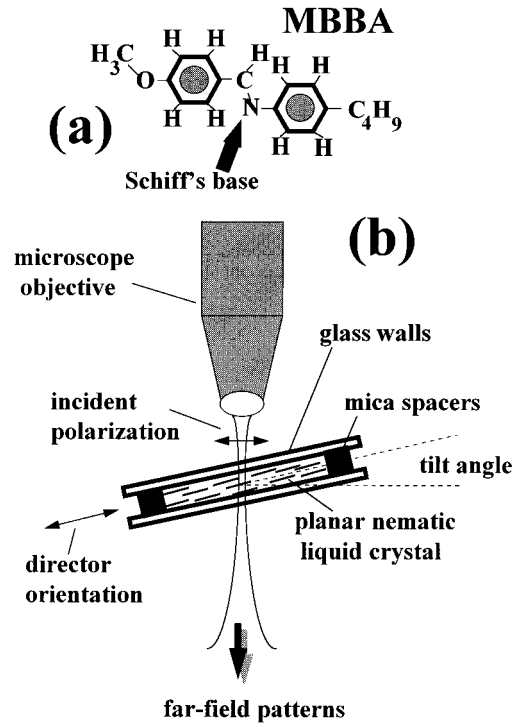


FIG. 1. (a) Schematic molecular structure of MBBA. The two benzene rings are joined by a relatively rigid backbone $CH=N$ called Schiff's base. The Raman modes of the latter are studied in connection with SRS. The molecule has also a comparatively flexible tail formed by the chain C_4H_9 . The lowest highest occupied molecular orbital to lowest unoccupied molecular orbital optical transition is for polarization roughly parallel to the main axis of the molecule at $\sim 400 \text{ nm} \sim 3.1 \text{ eV}$. MBBA is transparent at the 514.5 nm green Ar^+ -laser line. (b) Experimental setup: a $10\times$ microscope objective focuses the light onto a $100\text{-}\mu\text{m}$ -thick nematic liquid crystal cell with planar alignment. The cell can be tilted to vary the angle between the director and the incident polarization, thus varying the onset of self-focusing and SRS. The far-field diffraction patterns of the 514.5-nm Ar^+ -laser light are observed in transmission. See text for further details.

ever, the diffraction pattern produced by a nonlinear film can be greatly simplified. It has been shown [1,60–62] that the phase modulation of the beam produced by (14) forms in the far field a diffraction pattern with a radial $I(r)$ intensity distribution given by a Kirchhoff diffraction integral of the form

$$I(r^*) \sim \left| \int_0^\infty r J_0(\gamma_1 r r^*) e^{-\gamma_2 r^2 - i[\phi_1(r) + \phi_2(r)]} dr \right|^2, \quad (16)$$

where $\phi_1(r) \sim r^2$, $\phi_2(r) \sim \exp(-\gamma_3 r^2)$, and $\gamma_{1,2,3}$ are constants. Equation (16) displays a series of characteristic aberrational rings in the far field. Indeed, since the nonlinearity in (14) is proportional to $I \sim E^2$ this phenomenon had been known from materials with a strong dependence of the optical constants on temperature (like some lead glasses) [63], although the effect is in this case insensitive to polarization. The aberrational rings in the diffracted beam can be used as a clear indication of self-phase-modulation and self-focusing in the liquid crystal. A fairly good estimation of the number of expected rings given by (16) can also be obtained by decomposing the input beam in plane waves and using the

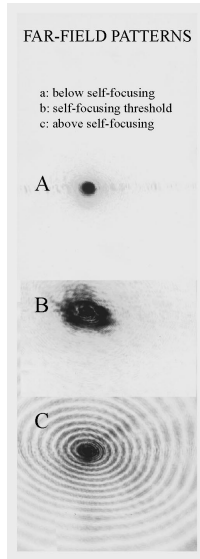


FIG. 2. Far-field patterns at a tilt angle of $\Theta = 15^\circ$ for intensities below (a), at (b), and above (c) the Fréedericksz transition. The incident polarization of the beam is in the plane defined by \vec{k}_L and \vec{n} and produce an optical torque $(15) \neq 0$. In (b) the beam is divergent and unstable in time at the threshold. In (c) the aberration rings produced by the self-phase-modulation of the beam (16) are clearly seen. Under normal conditions we can observe up to ~ 30 rings at the highest power density attainable.

method of the stationary phase [9]. If the initial beam is tightly focused and cannot be approximated by a plane wave the interaction of the elastic energy of the liquid crystal on the periphery of the beam also plays a role in the nonlinear interaction [13]. We ignore the latter for our experimental conditions.

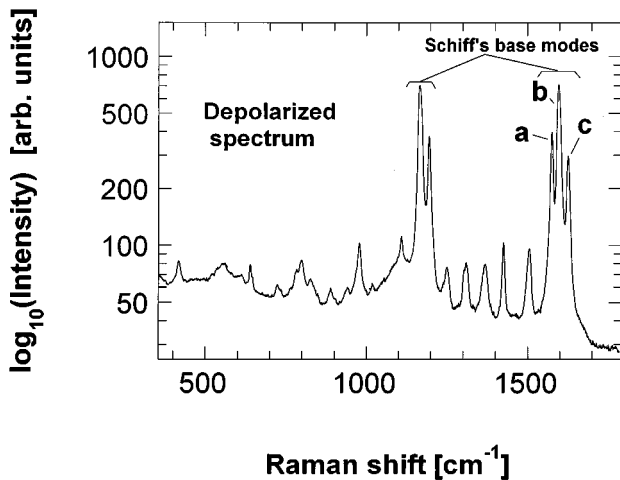


FIG. 3. Depolarized Raman spectrum of a multidomain (unoriented) drop of MBBA at room temperature. The Schiff's base modes are the dominant features of the spectrum (note the logarithmic scale). We concentrate in the upper modes labeled *a*, *b*, and *c* for the SRS experiments. The spectrum is a superposition of five spectra covering a range of $\sim 300 \text{ cm}^{-1}$ each, with the multichannel spectrometer at a resolution of $\sim 2 \text{ cm}^{-1}$ and with a fixed integration time of 30 sec.

III. EXPERIMENT

In Fig. 1(a) we show the molecular structure of MBBA [3]. The two benzene rings are joined by a relatively rigid backbone $CH=N$ called Schiff's base. The molecule has a flexible tail of C_4H_9 attached to one of the benzene rings. We shall concentrate on modes associated with the rigid backbone in what follows. Raman experiments were performed in a backscattering configuration using a micro-Raman DILOR multichannel setup at a constant temperature of 24°C (where MBBA is nematic). A schematic view of the setup is given in Fig. 1(b). A $10\times$ microscope objective focuses the input 514.5-nm green Ar^+ -laser light to a waist of $10 \mu\text{m}$ and into the liquid crystal cell. The reason for using a microscope is threefold: (i) It allows us to reach power densities that are useful for our experiment; (ii) it gives access to a fairly accurate positioning of the focus inside the cell (the limiting surfaces of the windows can be clearly seen in the microscope); and (iii) it permits the selection of a defect-free domain of the nematic avoiding problems caused by small dust particles or air bubbles trapped inside the cell. The focus of the beam is placed close to the first window inside the cell.

The alignment of the molecules is produced by rubbing the glass walls with $0.3\text{-}\mu\text{m}$ -grain size diamond paste [64]. The two windows are separated by a $100\text{-}\mu\text{m}$ mica spacer. The uniformity of the alignment was checked by observing the conoscopic patterns [3] through crossed polarizers. The cell can be tilted as shown in Fig. 1(b) up to $\Theta \sim 20^\circ$ in order

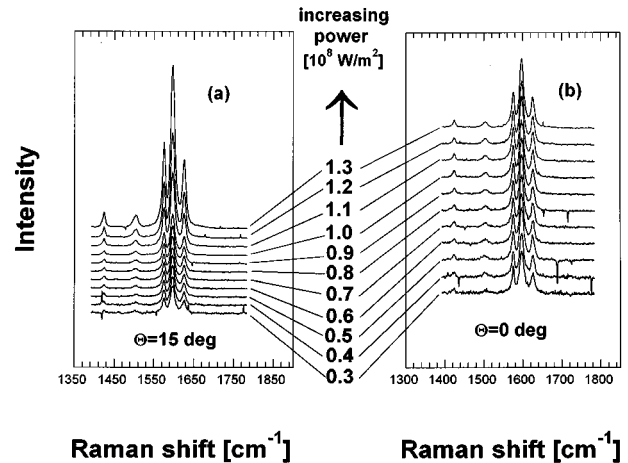


FIG. 4. Normalized Raman spectra of the modes in Fig. 3 for two different tilt angles Θ and orientations of the initial polarization. In (a) the incident polarization is in the plane containing \vec{k}_L and \vec{n} and the cell has a tilt angle $\Theta = 15^\circ$. The scattered light is analyzed with polarization $\vec{e}_s \parallel \vec{e}_i$, i.e., except for the small tilt angle of the cell the scattering efficiency is roughly I_{zz} [see (2)]. The torque (15) is different from zero under this condition and above a certain critical power density a Fréedericksz transition occurs. The normalized Raman scattering cross section remains almost constant up to this threshold in which it increases exponentially. In (b) the cell is at $\Theta = 0$ and the incident polarization is perpendicular to the plane defined by \vec{k} and \vec{n} . In this situation self-focusing does not take place and the normalized Raman cross section remains approximately constant. The latter demonstrates a negligible contribution from heating due to residual absorption in our experiments.

to change the angle of the incident beam with respect to the director. The far-field diffracted patterns transmitted through the cell are reflected through a mirror and projected onto a screen at ~ 1 m from the cell where they can be photographed.

Figure 2 shows an example of the far-field diffracted patterns below, at, and above the Freedericksz transition. In Fig. 2(a) the intensity is well below the critical value and the internal elastic energy of the liquid crystal dominates. In Fig. 2(b) the beam starts to show a considerable divergence and is unstable in time with a typical response of a few seconds. Finally, Fig. 2(c) shows the situation above the Fréedericksz transition where the aberrational rings given by (16) are clearly seen. It is therefore quite easy to determine whether self-focusing is taking place inside the cell. The typical response time for the ring formation is again of a few seconds.

We now turn to the Raman scattering data with and without self-focusing. In Fig. 3 we show the depolarized Raman spectrum in a multidomain drop of MBBA at room temperature and low excitation power [41]. The spectrum is dominated by five modes (note the logarithmic scale in Fig. 3), which are known to come from the Schiff's base [41]. Their Raman polarizability tensors are diagonal as in (1) along of the main directions of the molecule. These modes have been used in the past [41,42] to obtain information on the nematic order parameter in the framework of the explanation given in

Sec. II A. We concentrate on the three upper modes at ~ 1575 , 1596 , and 1626 cm^{-1} because we can measure them simultaneously with the multichannel detector and long integration times and also because of their large scattering cross sections. These modes have been labeled *a*, *b*, and *c* in Fig. 3. The rest of the spectrum shows a complex structure of molecular modes, which were studied in some detail in Ref. [44]. An interesting characteristic of the Raman spectrum of MBBA is the appearance of some weak modes according to the phase in which the liquid crystal is observed. The latter effect is partly due to the modifications in the structure produced by the molecular field of the different mesophases [45]. Actually, the low-energy part of the inelastic scattering spectrum up to ~ 200 cm^{-1} is remarkably sensitive to the liquid crystalline phase. The modes we monitor here for SRS are free from this problem.

Figure 4 displays a typical sequence of normalized Raman spectra of the modes *a*, *b*, and *c* in Fig. 3 in two different situations. In Fig. 4(a) the tilt angle is $\Theta = 15^\circ$ and \vec{E}_L is in the plane defined by \vec{n} and \vec{k}_L producing a torque $\vec{M}_{\text{opt}} \neq 0$ in (15). The normalized Raman intensity remains constant up to a critical value where all the modes increase exponentially with the pump power. A very different situation is achieved in Fig. 4(b) where $\Theta = 0^\circ$ and \vec{E}_L is perpendicular to both \vec{n} and \vec{k}_L . The normalized intensity remains approximately

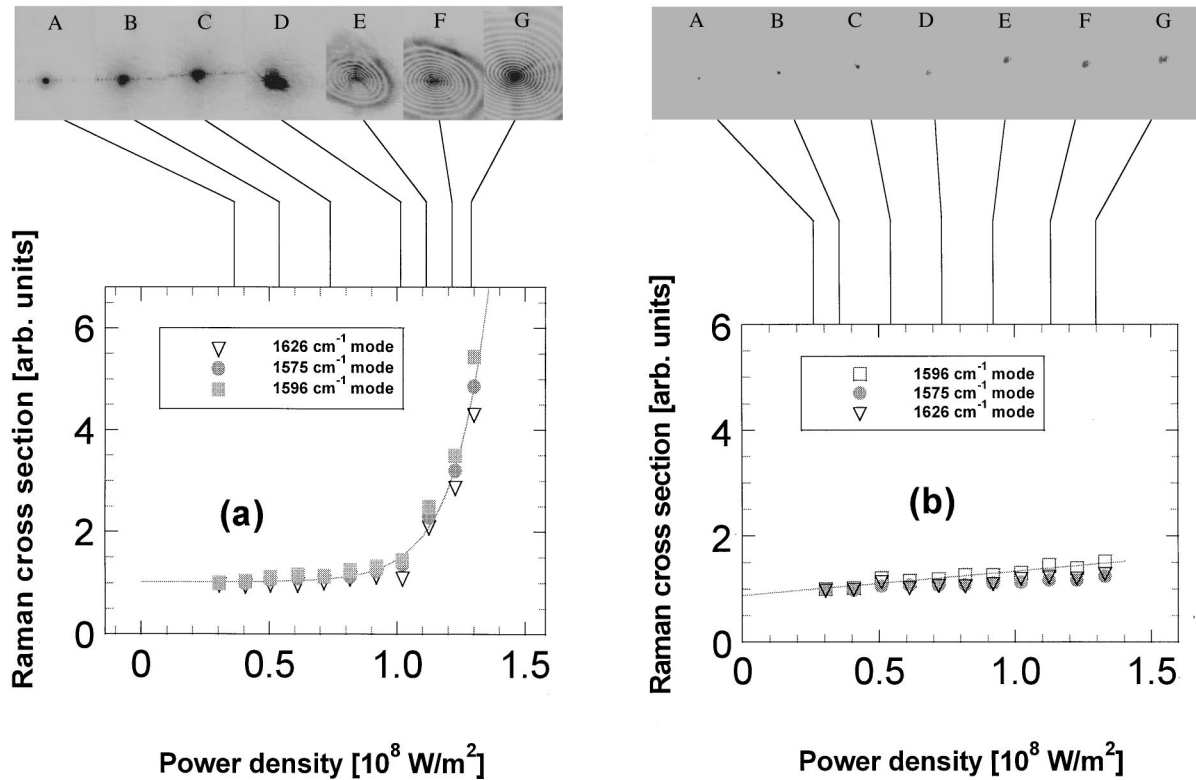


FIG. 5. Normalized Raman scattering cross sections for the modes labeled in Fig. 3. The data for the different peaks are divided by their intensity at low power densities so that they all lay on a common curve. In (a) \vec{E}_L is in the plane of \vec{n} and \vec{k}_L and the tilt angle [see Fig. 1(b)] is $\Theta = 15^\circ$. The far-field patterns of the transmitted light are shown simultaneously. At $\sim 1.0 \times 10^8$ W/m 2 (photo D) the beam becomes unstable and shows thereafter aberration rings for higher power densities. This coincides with the onset of SRS in the Raman data. In (b) we show data for the same power densities but with \vec{E}_L perpendicular to both \vec{n} and \vec{k}_L . The scattering is analyzed as in Fig. 4 with $\vec{e}_s \parallel \vec{e}_i$ and corresponds exactly to $I_{xx} = I_{yy}$ in (2). There is a small divergence of the far field causing probably the small drift of the cross section but neither self-focusing nor SRS is observed, in sharp contrast with case (a). See text for further details.

constant in the latter case where optical reorientation is not produced and shows, by the same token, a negligible possible effect of heating through residual absorption. The proportionality constant in (15) $C \propto \Delta \varepsilon = (\varepsilon_{\parallel} - \varepsilon_{\perp})$ is >0 in the optical range for MBBA; i.e., the interaction with the light is minimized when the long axis of the molecule is parallel to \vec{E}_L . One would therefore naively expect the situation $\vec{E}_L \perp \vec{n}$ to be unstable and expect optical reorientation, probably in a longer time scale, triggered by small departures or fluctuations of \vec{n} with respect to \vec{E}_L . This is not so in nematics and the explanation for it is both simple and subtle: the absence of optical reorientation for \vec{E}_L perpendicular to the director (although energetically unstable) is related to the *adiabatic propagation of light* and has been thoroughly treated by Csillag *et al.* [65]. For our purposes here we can always use this case to avoid self-focusing and have a test measurement.

As a matter of fact, we can observe directly the relation between the Raman spectra and self-focusing by putting together both the far-field transmitted patterns of the laser and the Raman scattering cross sections of the data in Fig. 4. This is done in Figs. 5(a) and 5(b) for the same experimental conditions of Figs. 4(a)–4(b). Since the peaks have different cross sections we normalize the data for the different peaks by the intensity at the lowest power density bringing all the data points to a common curve. In Fig. 5(a) the far field patterns show an increasing divergence of the beam until it becomes unstable at $\sim 1.0 \times 10^8 \text{ W/m}^2$ (photograph D). Above that threshold the aberrational rings are clearly seen in the far fields (photographs E, F, and G) implying that self-focusing is taking place inside the cell. The effect is coincident with the observed threshold for SRS of the modes. Conversely, Fig. 5(b) for $\vec{E}_L \perp \vec{k}_L$ and \vec{n} and $\Theta = 0^\circ$ a very small increase in the divergence of the beam is observed (probably due to small deviations from perfect orthogonality of \vec{E}_L with respect to \vec{n}). This small divergence in the far field implies a tiny tendency to self-focusing inside the cell, which probably causes the small, but monotonic, increase of the cross sections in Fig. 5(b). In any case, neither a Fréedericksz transition nor a SRS threshold is observed in this second instance and the contrast with Fig. 5(a) is explicit.

Since the Fréedericksz transition threshold depends on (15) reaching a given value, we can change the power density we actually need to attain self-focusing by changing the angle of the cell. From (15) we have $\vec{M}_{\text{opt}} \propto E_L^2 \sin(\Theta) \cos(\Theta)$ and the threshold for SRS and self-focusing is expected to change from $1.0 \times 10^8 \text{ W/m}^2$ at $\Theta = 15^\circ$ to $\sim 1.5 \times 10^8 \text{ W/m}^2$ if $\Theta = 5^\circ$. This is shown in Fig. 6 where the normalized scattering cross sections for the modes labeled in Fig. 3 are measured for the two angles mentioned. The shift in the SRS threshold is in excellent accord with the prediction.

An additional proof can be made to verify that effectively the exponential increase in the scattering cross section is due to SRS. To this end, we can observe the second-order Raman scattering spectra of the modes under consideration. The second-order spectra are expected to show a small but perceptible enhancement above the SRS threshold due to the superposition of the overtones of the Stokes Raman scattering. We explain briefly the reason for this in Fig. 7 where we

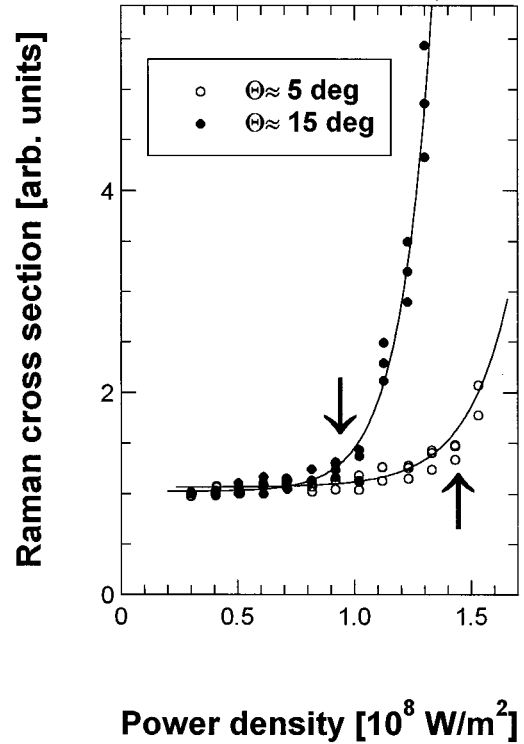


FIG. 6. Normalized Raman cross sections for the modes in Fig. 4 for \vec{E}_L in the plane of \vec{n} and \vec{k}_L and two different tilt angles, $\Theta = 15^\circ$ and 5° . By changing the angle a larger field intensity is needed for $\Theta = 5^\circ$ to achieve the Fréedericksz transition threshold and, therefore, self-focusing and SRS. The quantitative change between the two thresholds (shown with vertical arrows) is in fairly good agreement with the reduction in the torque predicted by (15).

show the Feynman diagrams of the Raman processes as self-energies of the laser photons. The first-order Raman scattering process, for example, is represented therefore in Fig. 7(a) as an incoming photon at ω_L creating an electron-hole pair (dashed bubble) and the subsequent emission of a vibration (phonon) at ω_p . The diagram is followed by its conjugate so that the total process represents the propagator of the photon with its inelastic interactions. The second-order Raman Feynman diagram is given on the right of Fig. 7(b) and in this case two vibrations are emitted from the electron-hole bubble via the electron-two-phonon interaction. On the other hand, it is also possible to have inelastic scattering at $2\omega_p$ through the diagram on the left of Fig. 7(b). In the latter, a Stokes photon created in a Raman process produces a first-order Raman scattering by itself. The second diagram is under normal circumstances negligible with respect to the first one and represents the overtone of the first-order Stokes scattering. The situation is quite the contrary under stimulated conditions in which the population of Stokes photons increases sharply. In fact, the second diagram can be as important as the first one (which is normally weak in any case) and an enhancement of the second-order spectra should be observed. The same holds for higher-order Raman processes although the effect is obviously weaker the higher the order.

In Fig. 8 we show the normalized second-order Raman spectra of the modes in Figs. 4 and 5 for the conditions of

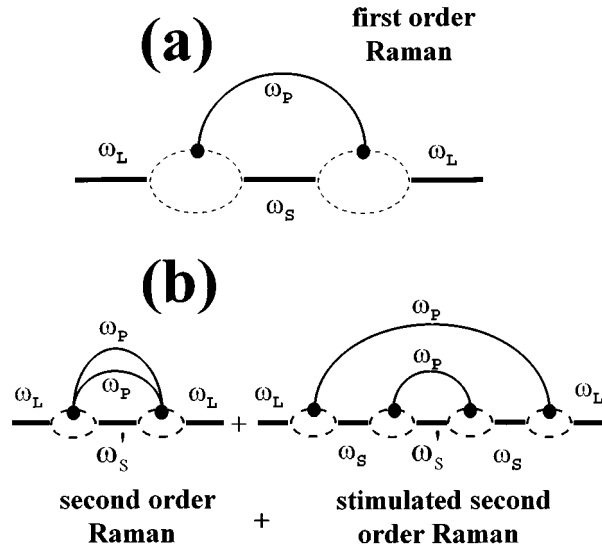


FIG. 7. (a) First-order Raman diagram. The thick horizontal lines represent the photon propagators while the continuous thin lines are the molecular vibrations. Dashed lines represent electron-hole pairs, which are virtual excitations if the laser is below the absorption edge. The diagram is put together with its conjugate and represents the self-energy $\hat{\omega}_{ph}$ of the photons with their inelastic interactions. The Raman spectra is given by $\sim -\text{Im}(\hat{\omega}_{ph})$. (b) Second-order Raman Feynman diagram (right) and stimulated second-order Raman (left). The second diagram represents the overtones of the first-order Raman and is normally negligible when the number of photons in the laser beam n_L greatly outnumbers the Stokes photons n_S , in other words, in normal Raman scattering conditions. In SRS, however, the two diagrams can be comparable in intensity and therefore an enhancement of the second-order signal is expected above threshold.

Fig. 5(a). We can again identify the presence or absence of self-focusing through the far-field images and determine the threshold of the Fréedericksz transition, which occurs at $1.0 \times 10^8 \text{ W/m}^2$ as in Fig. 5(a) (shown with a horizontal line in Fig. 8). The bump between ~ 3150 and 3225 cm^{-1} is the second-order Raman spectrum of the peaks shown in Figs. 4 and 5. There is a clear enhancement of the signal above threshold, as expected, giving further evidence for a SRS phenomenon. In fact, the three modes under study should produce three overtones each, not only enhancing the second-order Raman spectrum but also producing an additional broadening, which is barely seen in Fig. 8 because of the intrinsic weakness of the signal.

IV. DISCUSSION AND CONCLUSIONS

There are two different (but connected) effects influencing the Raman signal when optical reorientation occurs. If the incident and scattered polarizations are not along the main axes of the nematic domain the cross section $I \sim |\vec{e}_i \cdot \hat{R} \cdot \vec{e}_s|^2$ is none of the ones used in (2). The correct value for the initial cross section at low-power densities must be obtained by rotating the Raman tensor (1) to a new system of axes. When the intensity is increased and the Fréedericksz transition threshold reached, two effects coexist: (i) The laser

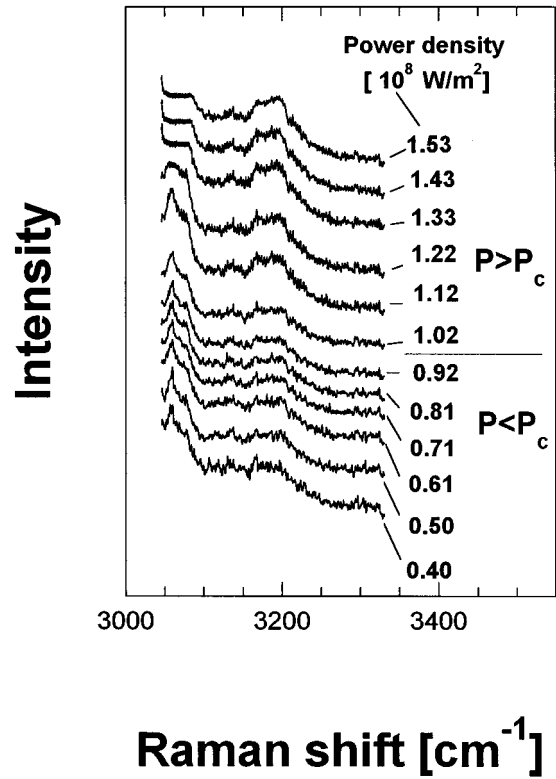


FIG. 8. Second-order Raman spectra for the conditions of Fig. 5(b). The presence of self-focusing is decided by the far-field patterns (not shown here) as in Fig. 5. The Fréedericksz transition occurs at a power density $P_c \sim 1.0-10^8 \text{ W/m}^2$ and is shown as a horizontal line separating two regimes $P < P_c$ and $P > P_c$. The broad peak between ~ 3150 and 3225 cm^{-1} is the second-order Raman of the modes in Fig. 4. A clear enhancement of the weak second-order signal is observed above P_c in accordance with SRS. A small change in the broadening of the spectra should also be expected due to the fact that each vibration creates three overtones. This is scarcely seen in the experiment due to the intrinsic weakness of the signal. Integration times here are $t \sim 10$ min to be compared with 30 sec for the first-order Raman in Figs. 3 and 4. See text for further details.

reorients the molecules and, strictly speaking, changes the Raman cross section by modifying the angle; i.e., by rotating the Raman tensor; and (ii) there is sudden increase in the power density produced by self-focusing, which, in turn, is also a consequence of the molecular reorientation producing the quadratic term in (14). The former effect, however, can be neglected with respect to the latter. Optical reorientation (without flow coupling [66]) can normally be solved in the context of the *small angle approximation* [2,67]. The reorienting angle $\Delta \theta$ follows a power law with respect to the pump beam [1] $\Delta \theta \sim E_L^2$ and, consequently, the change in the scattering cross section produced by a small rotation of the Raman tensor will also follow a power law to first order. This bears, accordingly, a small correction to the exponential dependence [see (12)] of the cross section for SRS, which dominates the effect. We believe that the evidence produced by the Raman data plus the far-field diffracted images and, in addition, the angle dependence of the threshold (Fig. 6) and the stimulated overtones on top of the second-order Raman (Figs. 7 and 8) gives a consistent picture of SRS in the nematic phase of MBBA.

Finally, very interesting possibilities should exist in Raman scattering from cholesterics [3] in the Bragg regime (optical wavelength \sim pitch). Cholesteric liquid crystals are a special kind of what we may call today a *photonic band material* [68]. In fact, cholesterics have a sharp stop band close to the Bragg condition for one of the two circular polarizations σ^+ or σ^- , depending on the helicity of the pitch [69]. A Raman process in backscattering with a cross section $I \sim |\sigma^+ \cdot \hat{R} \cdot \sigma^-|^2 \neq 0$ can be inhibited at the stop band and, in addition, induced untwisting of the pitch produced by external fields should breed a variety of possibilities with unique characteristics. Raman experiments in mixtures of chole-

teryl oleyl carbonate, cholesteryl nonanoate, and cholesteryl chloride, to produce variable pitches in the $\sim 1\text{-}\mu\text{m}$ regime according to the needs are in progress and will be reported elsewhere [70].

ACKNOWLEDGMENTS

Thanks are due to A. Fainstein (CNET-Telecom, France) for several comments on the manuscript. Pablo Etchegoin wishes to thank the European Union for financial support at the Cavendish Lab. in Cambridge (UK). This work has been supported by EPSRC (UK).

-
- [1] For a comprehensive review on the most important developments in the field see Iam-Choon Khoo, *Liquid Crystals, Physical Properties and Nonlinear Optical Phenomena* (Wiley, New York, 1995), p. 241.
- [2] Iam-Choon Khoo, in *Progress in Optics*, edited by E. Wolf (North-Holland, Amsterdam, 1988), Vol. 26, p. 105; see also N. V. Tabiryan, A. V. Sukhov, and B. Ya Zeldovich, *Mol. Cryst. Liq. Cryst.* **136**, 1 (1986).
- [3] For a general overview on the physical properties of the different liquid crystalline mesophases see the introductory chapters of P. G. deGennes, *The Physics of Liquid Crystals* (Clarendon Press, Oxford, 1974); L. M. Blinov, *Electro-Optical and Magneto-Optical Properties of Liquid Crystals* (Wiley, New York, 1983) and S. Chandrasekhar, *Liquid Crystals* (Cambridge University Press, New Rochelle, 1980). A useful review on early results can also be found in Michael J. Stephen and Joseph P. Straley, *Rev. Mod. Phys.* **46**, 617 (1974).
- [4] A gathering of the most relevant papers in linear and nonlinear optics of liquid crystals is given in *Optical Effects in Liquid Crystals*, edited by I. Jánossy (Kluwer Academic Publishers, Boston, 1991).
- [5] G. K. L. Wong and Y. R. Shen, *Phys. Rev. Lett.* **32**, 527 (1974).
- [6] A. S. Zolotko, V. F. Kitaeva, N. N. Sobolev, and A. P. Sukhorukov, *Zh. Éksp. Teor. Fiz.* **81**, 3 (1981) [*Sov. Phys. JETP* **54**, 495 (1981)].
- [7] I. C. Khoo, S. L. Zhuang, and Shepard, *Appl. Phys. Lett.* **39**, 937 (1981).
- [8] E. Santamato and Y. R. Shen, *Opt. Lett.* **9**, 564 (1985).
- [9] N. F. Pilipetski, A. V. Sukhov, N. V. Tabiryan, and B. Ya Zeldovich, *Opt. Commun.* **37**, 280 (1981).
- [10] A. S. Zolotko, V. F. Kitaeva, N. Kroo, N. N. Sobolev, and L. Chillag, *Pis'ma Zh. Éksp. Teor. Fiz.* **32**, 170 (1980) [*JETP Lett.* **32**, 158 (1980)].
- [11] S. D. Dubrin, S. M. Arakelian, and Y. R. Shen, *Phys. Rev. Lett.* **47**, 1411 (1981).
- [12] B. Ya Zeldovich, N. V. Tabiryan, and Yu. S. Chilingaryan, *Zh. Éksp. Teor. Fiz.* **81**, 72 (1991) [*Sov. Phys. JETP* **54**, 32 (1981)].
- [13] L. Csillag, I. Jánossy, V. F. Kitaeva, N. Kroo, and N. N. Sobolev, *Mol. Cryst. Liq. Cryst.* **84**, 125 (1982).
- [14] I. C. Khoo, T. H. Liu, and P. Y. Yan, *J. Opt. Soc. Am.* **4**, 115 (1987).
- [15] E. Santamato, G. Abbate, P. Maddalena, and Y. R. Shen, *Phys. Rev. A* **36**, 2389 (1987).
- [16] For optical induced molecular reorientations in a smectic mesophase see Hiap Liew Ong and Charles Y. Young, *Phys. Rev. A* **29**, 297 (1984).
- [17] Erez Braun, Luc P. Faucheux, and Albert Libchaber, *Phys. Rev. A* **48**, 611 (1993).
- [18] P. A. Madden, F. C. Saunders, and A. M. Scott, *IEEE J. Quantum Electron.* **22**, 1287 (1986).
- [19] F. Sanchez, P. H. Kayoun, and J. P. Huignard, *J. Appl. Phys.* **64**, 26 (1988).
- [20] I. C. Khoo and T. H. Liu, *Phys. Rev. A* **39**, 4036 (1989).
- [21] J. W. Shelton and Y. R. Shen, *Phys. Rev. Lett.* **25**, 23 (1970); *Phys. Rev. A* **5**, 1867 (1972).
- [22] S. K. Saha and G. K. Wong, *Opt. Commun.* **30**, 119 (1979).
- [23] J. Y. Liu, M. G. Robinson, K. M. Johnson, D. M. Wabba, M. B. Ros, N. A. Clark, R. Shao, and D. Doroski, *Opt. Lett.* **15**, 267 (1990).
- [24] I. C. Khoo and S. L. Zhuang, *IEEE J. Quantum Electron.* **18**, 246 (1981).
- [25] M. I. Barnik, L. M. Blinov, A. M. Dorozhkin, and N. M. Shtykov, *Mol. Cryst. Liq. Cryst.* **98**, 1 (1983).
- [26] B. Ya Zeldovich and N. V. Tabiryan, *Kvantovaya Elektron (Moscow)* **7**, 770 (1980) [*Sov. J. Quantum Electron.* **10**, 440 (1980)].
- [27] A. V. Sukhov, *Mol. Cryst. Liq. Cryst.* **185**, 227 (1990)
- [28] B. Ya Zeldovich, S. K. Merslikin, N. F. Pilipetsky, and A. V. Sukhov, *Pis'ma Zh. Éksp. Teor. Fiz.* **41**, 418 (1985) [*JETP Lett.* **41**, 514 (1985)].
- [29] I. C. Khoo, H. Li, and Yu Liang, *Opt. Lett.* **18**, 3 (1993).
- [30] D. N. Ghosh Roy and D. V. G. L. N. Rao, *J. Appl. Phys.* **59**, 332 (1986).
- [31] Z. K. Ioannidis, I. P. Giles, and C. Bowry, *Appl. Opt.* **30**, 328 (1991).
- [32] E. S. Goldburt and P. St. J. Russell, *Appl. Phys. Lett.* **46**, 338 (1985).
- [33] I. C. Khoo, J. Y. Hou, R. Normandin, and V. C. Y. So, *Phys. Rev. A* **27**, 3251 (1983).
- [34] M. M. Cheung, S. D. Dubrin, and Y. R. Shen, *Opt. Lett.* **8**, 39 (1983).
- [35] I. C. Khoo, Ping Zhou, R. R. Michael, R. G. Lindquist and R. J. Mansfield, *IEEE J. Quantum Electron.* **25**, 1755 (1989).
- [36] S. R. Nersisyan and N. V. Tabiryan, *Mol. Cryst. Liq. Cryst.* **116**, 111 (1984).

- [37] H. G. Winful, *Phys. Rev. Lett.* **49**, 1179 (1982).
- [38] Hiap Liew Ong, *Appl. Phys. Lett.* **46**, 822 (1985).
- [39] A. D. Lloyd and B. S. Wherrett, *Appl. Phys. Lett.* **53**, 460 (1988).
- [40] Purchased from Frinton Labs. (USA).
- [41] Shen Jen, Noel A. Clark, P. S. Pershan, and E. B. Priestley, *J. Chem. Phys.* **66**, 4635 (1977).
- [42] K. Miyano, *J. Chem. Phys.* **69**, 4807 (1978).
- [43] Yuko Nakajima, Hiroshi Yoshida, Shunsuke Kobinata, and Shiro Maeda, *J. Phys. Soc. Jpn.* **49**, 1140 (1980).
- [44] C. Destrade and H. Gasparoux, *J. Phys. (Paris) Lett.* **36**, L-105 (1975).
- [45] Iam-Choon Khoo and Shin-Tson Wu, *Optics and Nonlinear Optics of Liquid Crystals* (World Scientific, London, 1993), p. 282.
- [46] For a brief introduction on Raman in molecules (in particular to symmetry aspects of the Raman tensors) see M. Cardona, in *Light Scattering in Solids II*, edited by M. Cardona and G. Güntherodt (Springer, Berlin, 1982), p. 29.
- [47] W. Maier and A. Saupe, *Z. Naturforsch.* **14A**, 882 (1959).
- [48] Groupe d'Etude des Cristaux Liquides (Orsay), *J. Chem. Phys.* **51**, 816 (1969). The strong scattering produced by the director fluctuations is, in fact, used to trigger optical phase conjugation by stimulated orientational scattering; see I. C. Khoo, Yu Liang and H. Li, *Opt. Lett.* **20**(2), 130 (1995).
- [49] A. Yariv, *Quantum Electronics* (Wiley, New York, 1989).
- [50] Y. R. Shen, *Principles of Nonlinear Optics* (Wiley, New York, 1984).
- [51] B. E. A. Saleh and M. C. Teich, *Fundamentals of Photonics* (Wiley, New York, 1991), p. 762.
- [52] V. Degiorgio and M. O. Scully, *Phys. Rev. A* **2**, 1170 (1970); R. Graham and H. Haken, *Z. Phys* **237**, 31 (1970).
- [53] M. Lax and W. H. Louisell, *Phys. Rev.* **185**, 568 (1969).
- [54] For a review of this and other related concepts in nonlinear optics see H. Haken, *Rev. Mod. Phys.* **47**, 67 (1975) and also H. Haken, *Light*, Vol. 2 (Laser Light Dynamics) (North-Holland, Amsterdam, 1985).
- [55] R. Y. Chiao, E. Garmire, and C. H. Townes, *Phys. Rev. Lett.* **13**, 479 (1964).
- [56] P. L. Kelley, *Phys. Rev. Lett.* **15**, 1005 (1965).
- [57] Y. R. Shen and Y. J. Shaham, *Phys. Rev. Lett.* **15**, 1008 (1965).
- [58] P. Lallemand and N. Bloembergen, *Phys. Rev. Lett.* **15**, 1010 (1965).
- [59] P. M. Chaikin and T. C. Lubensky, *Principles of Condensed Matter Physics* (Cambridge University Press, Cambridge, 1995); see also Refs. [55] for a general introduction to critical slowing down in second-order phase transitions and in laser dynamics.
- [60] I. C. Khoo, J. Y. Hou, T. H. Liu, P. Y. Yan, R. R. Michael, and G. M. Finn, *J. Opt. Soc. Am. B* **4**, 886 (1987).
- [61] I. C. Khoo, P. Y. Yan, T. H. Liu, S. Shepard, and J. Y. Hou, *Phys. Rev. A* **29**, 2756 (1984).
- [62] A related effect is the diffraction patterns produced by a thin nematic film with planar orientation but with two incident lasers (creating a grating) and has been studied in S. J. Elston, D. J. Webb, and L. Solymar, *Phys. Rev. B* **48**, 1172 (1993).
- [63] F. W. Dabby, T. K. Gustafson, J. R. Whinnery, and Y. Kohanzadel, *Appl. Phys. Lett.* **16**, 362 (1970).
- [64] P. Chatelain, *Bull. Soc. fr. Minér.* **66**, 105 (1943); J. L. Lanning, *Appl. Phys. Lett.* **21**, 15 (1972); D. Berreman, *Phys. Rev. Lett.* **28**, 1683 (1972).
- [65] L. Csillag, I. Jánossy, V. F. Kitaeva, N. Kroó, N. N. Sobolev, and A. S. Zolotko, *Mol. Cryst. Liq. Cryst.* **78**, 173 (1981).
- [66] H. J. Eichler and R. Macdonald, *Phys. Rev. Lett.* **67**, 2666 (1991).
- [67] R. M. Herman and R. J. Serinko, *Phys. Rev. A* **19**, 1757 (1979).
- [68] E. Yablonovitch, *Phys. Rev. Lett.* **58**, 2059 (1987).
- [69] Hl. de Vries, *Acta Crystallogr.* **4**, 219 (1951).
- [70] P. Etchegoin and R. T. Phillips (unpublished).
- [71] There is a previous report of SRS using a pulsed ruby laser in D. V. G. L. Narasimha Rao and D. K. Agrawal, *Phys. Lett.* **37A**, 383 (1971), but no specific relation to the phenomenon of self-focusing is mentioned here.